Original Article

The dynamic contrast enhanced-magnetic resonance imaging and diffusion-weighted imaging features of alveolar soft part sarcoma

Changlei Lv[1#], Xiaolei Xue[2#], Minggang Huang[1], Zhen Yang[1], Xiaolong Chen[1], Chi Wan Koo[3]

[1]Department of Radiology, Shaanxi Provincial People's Hospital, Xi'an, China; [2]Department of Ultrasound, Shandong Provincial Third Hospital, Shandong University, Jinan, China; [3]Department of Radiology, Mayo Clinic, Rochester, MN, USA

Contributions: (I) Conception and design: X Xue; (II) Administrative support: M Huang; (III) Provision of study materials or patients: Z Yang, X Chen; (IV) Collection and assembly of data: C Lv; (V) Data analysis and interpretation: X Xue, C Lv; (VI) Manuscript writing: All authors; (VII) Final approval of manuscript: All authors.

[#]These authors contributed equally to this work.

Correspondence to: Xiaolei Xue, PhD. Department of Ultrasound, Shandong Provincial Third Hospital, Shandong University, 12 Wuyingshan Road, Tianqiao District, Jinan 250031, China. Email: shiley_xue@163.com.

Background: Alveolar soft part sarcoma (ASPS) is a rare type of soft tissue sarcoma that predominantly affects adolescents and young adults. Early diagnosis of ASPS is crucial for optimal therapeutic planning and improving prognosis, but its diagnostic features are not well delineated. This study aimed to retrospectively analyze the imaging features of ASPS with an emphasis on the dynamic contrast-enhanced-magnetic resonance imaging (DCE-MRI) and diffusion-weighted imaging (DWI) findings to identify imaging findings that might suggest the diagnosis to radiologists.

Methods: The imaging features of 34 patients with pathologically proven limb ASPS were retrospectively analyzed. A total of 23 underwent DCE-MRI, and 12 underwent DWI.

Results: Among the 34 cases of ASPS, 31 tumors were in the lower extremities, and 3 were in the upper extremities. The maximum tumor diameters ranged from 3.0 to 19.4 cm (mean, 8.7±3.96 cm). A total of 28 cases had well-defined borders. The masses demonstrated heterogeneous high signal intensity on T2-weighted imaging (T2WI) and the fat-suppressed (FS) T2WI sequence and slight hyperintensity on T1-weighted imaging (T1WI). A total of 25 lesions had thin hypointense bands on T1WI and T2WI. Intra- and peri-tumoral tubular areas of flow void were exhibited on both T1WI and T2WI in all cases. A total of 12 cases showed a high signal on DWI, and the mean apparent diffusion coefficient (ADC) value was $(0.86\pm0.07)\times10^{-3}$ mm^2/s [range, $(0.6–1.4)\times10^{-3}$ mm^2/s]. Persistent remarkable enhancement of the lesion was displayed on contrast-enhanced scans. The time-intensity curves (TICs) of 23 masses showed early arterial enhancement and slow washout of contrast.

Conclusions: ASPS most commonly presents in the lower extremities of adolescents or young adults. Hyperintense T1WI, T2WI, and DWI signals, low ADC, flow voids, early arterial enhancement are frequent MRI features.

Keywords: Alveolar soft part sarcoma (ASPS); magnetic resonance imaging (MRI); dynamic contrast-enhanced (DCE); diffusion-weighted imaging (DWI)

Submitted May 25, 2023. Accepted for publication Aug 25, 2023. Published online Sep 11, 2023.
doi: 10.21037/qims-23-743
View this article at: https://dx.doi.org/10.21037/qims-23-743

Introduction

Alveolar soft part sarcoma (ASPS) is a clinically and histopathologically distinct sarcoma that was first proposed by Christopherson *et al.* (1) in 1952. According to the 2013 World Health Organization (WHO) classification of soft tissue tumors, ASPS belongs to the category of malignant soft part tumors with uncertain differentiation (2). It is an extremely rare type of soft tissue sarcoma that predominantly affects adolescents and young adults. ASPS generally arises in skeletal muscles of lower limbs and needs to be differentiated from Ewing's sarcoma/embryonal tumor (ES/ET). ES/ET should be suspected in young adults presenting with a large heterogeneous mass in their extremities (3). Although ASPS is an indolent tumor, the hematogenous spread of the tumors to other tissues, usually pulmonary metastases, tends to occur early, indicating the aggressive behavior of ASPS and portends a poor prognosis. Radical surgical excision is the optimal treatment for patients with early-stage ASPS, as ASPS is resistant to radiotherapy and chemotherapy (4). If radically excised, local recurrence can be reduced, and long-term survival may be realizable (5). Thus, early diagnosis of ASPS, especially before metastasis, is crucial for optimal therapeutic planning and improving prognosis. Unfortunately, features of ASPS are not well delineated; it is often difficult to make an accurate diagnosis.

Diagnostic magnetic resonance imaging (MRI) plays an important role in lesion identification and characterization. The conventional imaging features of ASPS have been reported in previous literature (6,7), such as high or isointense signal on T1-weighted imaging (T1WI) and multiple signal voids highly suggestive of ASPS in MRI (8,9), but nonconventional MRI techniques are not widely studied. Gondim Teixeira *et al.* found that semi-quantitative magnetic resonance (MR) perfusion parameters provide information with regard to the degree of tumor necrosis in musculoskeletal sarcomas (10). Other nonconventional MRI techniques, including quantitative dynamic contrast enhanced (DCE)-MRI parameters and diffusion-weighted imaging (DWI), are closely related to clinical, histopathological, and prognostic factors of tumors (11). For example, DCE-MRI is considered the most effective modality currently available for assessing the response of high-grade osteosarcoma and ES to preoperative chemotherapy (12). Thus, the aim of our study was to retrospectively analyze the imaging features of ASPS with an emphasis on the DCE-MRI and DWI, to determine if there are features that suggest the diagnosis. We present this article in accordance with the MDAR reporting checklist (available at https://qims.amegroups.com/article/view/10.21037/qims-23-743/rc).

Methods

The present study was approved by the Ethics Committee of Shaanxi Provincial People's Hospital (No. 2021X012) and was conducted in accordance with the Declaration of Helsinki (revised in 2013). The requirement for informed consent was waived because of the study's retrospective nature. A total of 34 patients with pathologically proven ASPS between June 2008 and July 2020 from Shaanxi Provincial People's Hospital were enrolled in this study. All 34 patients underwent unenhanced MR scan, 23 underwent additional DCE-MRI, 12 underwent additional DWI, and 3 underwent computed tomography angiography (CTA).

All MRI examinations were performed using 1.5- or 3.0-T MR system (Ingenia 1.5T and 3.0T; Philips, Best, Netherlands). MRI scan protocols are summarized in *Table 1*. DCE-MRI was performed using an e-THRIVE_dyn_BH Sensitivity Encoding (SENSE) sequence in the axial plane [flip angle, 10°; repetition time (TR), 2–3 ms, echo time (TE), 1 ms; slice thickness, 6–7 mm; interslice gap, 0 mm; field of view (FOV), 200 mm × 295 mm; matrix size, 285×512 pixels; parallel reduction factor, 2]. Before administration of contrast medium, precontrast T1-weighted fast field echo sequences (flip angle: 5°, 10°, and 15°) were applied in the same geometry to calculate baseline T1 maps using the same axial 3-dimensional (3D) fast field echo sequence. DCE-MRI was obtained immediately after injecting a bolus of gadobutrol (Bayer, Berlin, Germany) at an injection flow rate of 3.0 mL/s and a dose of 0.1 mmol/kg, followed by a 15 mL flush of normal saline. DCE-MRI included 12 dynamic volume images with a temporal resolution of 12 seconds obtained over 5 minutes. Axial and coronal fat-suppressed (FS) T1-weighted images were collected after DCE-MRI. The time-intensity curve (TIC) of the ASPS lesion, adjacent muscles, and arteries at the same level were obtained by dynamic enhancement analysis software in a dedicated workstation. Spin-echo echo planar imaging (SE-EPI) sequence was used for DWI. The b-values were taken as 0 and 800 s/mm^2 and the corresponding apparent diffusion coefficient (ADC) was obtained. The ADC was calculated by selecting the region of interest (ROI) (*Figure 1*)

Table 1 Acquisition parameters of MRI protocols

Parameters	Plain scan				DCE-THRIVE (enhanced imaging)
	T1WI	T2WI	T2WI	DWI	
Sequence	TSE	TSE	TSE	SE-EPI	dyn-THRIVE
Scan direction	Transverse	Transverse	Transverse	Transverse	Transverse
Fold over direction	RL	RL	RL	RL	RL
Fat suppression	None	None	SPAIR	SPAIR	SPAIR
TR/TE (ms)	520/20	2,411/130	3,852/70	2,750/63	2–3/1
Flip angle (°)	90	90	90	90	10
Field of view (mm)	320×300	320×300	320×300	260×260	200×295
Voxel size (mm)	0.80×0.80	0.70×0.85	0.70×0.85	3.00×3.00	1.20×1.20
Slice thickness (mm)	4	4	4	4	6–7
Total acquisition time	2'5''	1'49''	2'17''	2'3''	4'50''

MRI, magnetic resonance imaging; T1WI, T1-weighted image; T2WI, T2-weighted image; DWI, diffusion-weighted imaging; DCE, dynamic contrast enhanced; THRIVE, T1-weighted high resolution isotropic volume examination; TSE, turbo spin echo; SE-EPI, spin-echo echo planar imaging; dyn-THRIVE, dynamic THRIVE; RL, right to left; SPAIR, spectral attenuated inversion recovery; TR, repetition time; TE, echo time.

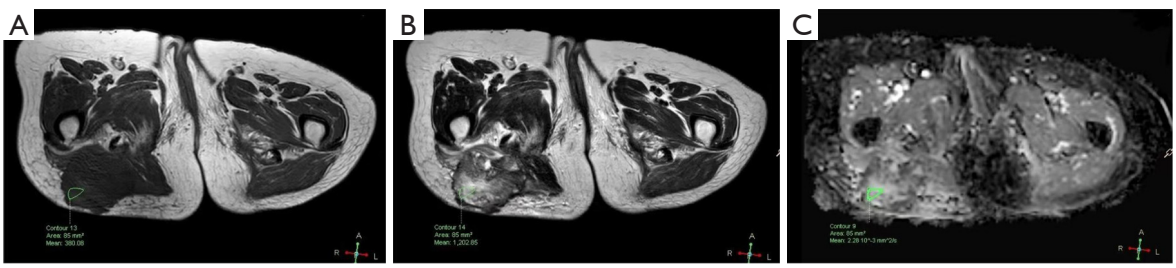

Figure 1 Illustration of ROI placement for ADC calculation. An ROI was placed on the T1-weighted image (A) and T2-weighted image (B), which automatically generated the ADC value of the lesion and was mapped on the ADC map (C, green elliptical region). A, anterior; R, right; L, left; ROI, region of interest; ADC, apparent diffusion coefficient.

by a radiologist with more than 5 years of experience (Chen X), excluding the vascular flow void area in the lesion as much as possible. The ADC was measured 3 times, and the average value was taken. Total collection time for each patient was approximately 13 to 14 minutes.

The computed tomography (CT) scans were performed with a Canon Aquilion^{TM} Vision 640 helical CT system (Canon, Otawara, Japan). A total of 3 patients were imaged with CTA. The main imaging parameters were as follows: section thickness reconstructions, 5 mm; FOV, 25 cm; tube voltage, 120 kV; current, 300 mA; and matrix, 512×512. An intravenous bolus dose of nonionic iodinated contrast agent (1.5 mL/kg body weight, iodixanol) was administered at a rate of 4.5 mL/s. The original data package was sent to the postprocessing workstation, and CTA 3D images were obtained using vascular software.

Two senior radiologists (Chen X and Yang Z) with at least 10 years of experience reviewed all images, and reached a consensus if there were discrepancies. The location, tumor size, shape, margin, internal and peripheral structures, density/signal intensity, absence or presence of peri-tumoral and intratumoral flow voids, contrast enhancement pattern, and TIC of the tumor were analyzed.

All information was summarized using descriptive statistics expressed as the mean ± standard deviation or the median (interquartile range) as appropriate for continuous variables, and number (%) for categorical variables. Chi-squared tests were performed when comparing proportions across groups.

Table 2 Patient demographic and clinical information

Parameters	Values
Total cases	34
Age at diagnosis (years)	
Mean ± SD	23.50±6.36
Range	9–49
Gender, n (%)	
Male	23 (67.6)
Female	11 (32.4)
Chief complaints, n (%)	
Painless mass	25 (73.5)
Pain	9 (26.5)
Location, n (%)	
Lower extremities	31 (91.2)
Upper extremities	3 (8.8)
Right side	21 (61.8)
Left side	13 (38.2)
Metastasis, n (%)	19 (55.9)
Lungs	12
Lungs and liver	2
Lungs and bone	2
Lungs, adrenal, and brain	1
Lungs, liver, and adrenal	2
Follow-up (years), n (%)	13 (38.2)
Mean ± SD	6.50±5.66
Range	1–12
Outcome, n (%)	13 (38.2)
Alive	10
Died	3

SD, standard deviation.

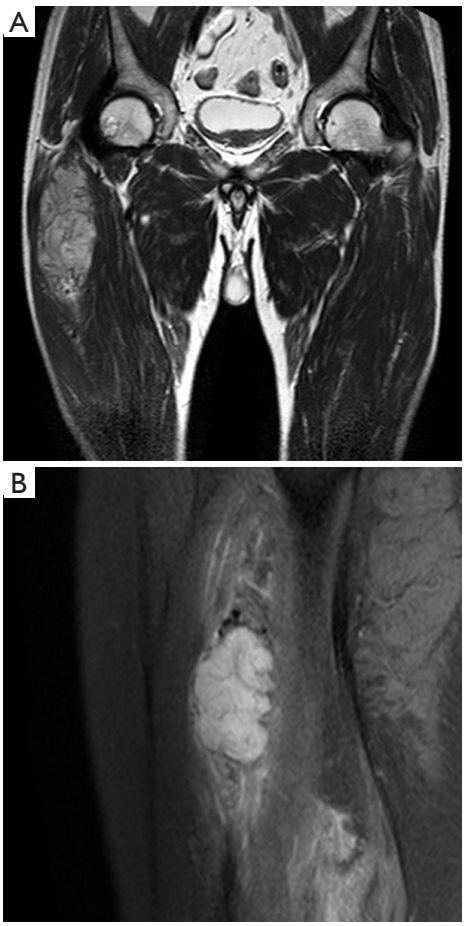

Figure 2 The tumors were performed on 3.0-T MRI scanner showed heterogenous high signal intensity compared with muscle on the coronal T2WI (A), and on the fat-suppressed sagittal T2WI (B). MRI, magnetic resonance imaging; T2WI, T2-weighted imaging.

Results

Clinical characteristics

Demographic and clinical information of the 34 patients is shown in *Table 2*. The tumors mainly presented as large masses. The maximum tumor diameters ranged from 3.0 to 19.4 cm (mean, 8.70±3.96 cm). A total of 21 masses were located on the right side, and 31 masses were in the lower extremities. The chi-square test showed that there were no significant differences in lesion locations (P=1). Masses appeared as round (n=10), ovoid (n=20), or irregular (n=4) shapes. A total of 28 cases had well-defined borders, and 6 cases had partially ill-defined margins.

Imaging features

For MRI, all the tumors showed heterogenous high signal intensity on T2-weighted imaging (T2WI) and FS sequence (*Figure 2*), and mildly hyperintense on T1WI (*Figure 3*) compared to adjacent muscle. A total of 5 of 34 (14.7%) tumors showed evidence of hemorrhage on T1WI (*Figure 4*). Thin hypointense bands within 25 cases were seen on T1WI and T2WI. Of the 34 cases, 32 showed multiple tortuous areas

of flow void on both T1WI and T2WI within the mas and along the lateral margins (*Figure 5*) and 2 cases showed such flow void in the peripheral margins. All 12 tumors (100%) that had undergone DWI showed high signal intensity, and the mean ADC value which showed normal distribution was $(0.86\pm0.07)\times10^{-3}$ mm^2/s [range, $(0.6–1.4)\times10^{-3}$ mm^2/s] (*Figure 6*). All 23 masses (100%) that had undergone DCE-MRI showed remarkable persistent enhancement compared with adjacent muscles (*Figure 7*). Tumors less than 10 cm in size (n=19) showed predominantly homogeneous postcontrast enhancement, whereas those greater than 10 cm (n=4) showed heterogeneous peripheral enhancement with a central hypoenhancing component. All 23 (100%) TIC demonstrated early arterial enhancement within the first 6 seconds and slow washout (*Figure 8*). A total of 3 cases were imaged with CTA, which demonstrated hypervascular masses with multiple enlarged tortuous vessels, as well as feeding arteries and draining veins in and out of the masses (*Figure 9*). Multiple lung metastases were found in 19 patients (19/34) at first diagnosis (*Figure 10A*). Lung metastases were found in another 1 patient 7 years after the operation, and the metastatic foci showed remarkable persistent enhancement (*Figure 10B*,*10C*). The imaging characteristics are summarized in *Table 3*.

Figure 3 The T1-weighted image shows a well-defined mass in the deep muscle, revealing slightly high signal intensity on 1.5-T MRI scanner. MRI, magnetic resonance imaging.

Discussion

The incidence of ASPS is low, accounting for less than 1% of all soft tissue sarcoma. Therefore, it is difficult to make an accurate diagnosis due to the limited experience with clinical characteristics. Previous studies have shown that ASPS mainly affects adolescents and young adults between the ages of 15 and 35 years (13,14). There is a slight female predominance in patients under the age of 30 years, whereas the opposite phenomenon has been found in patients above 30 (13). ASPS can occur in all body parts, mostly in the deep soft tissues of the thighs and buttocks in adults, whereas it is mainly found in the head and neck in infants and children, especially in the orbit and tongue (14,15). In agreement with previous observations, our

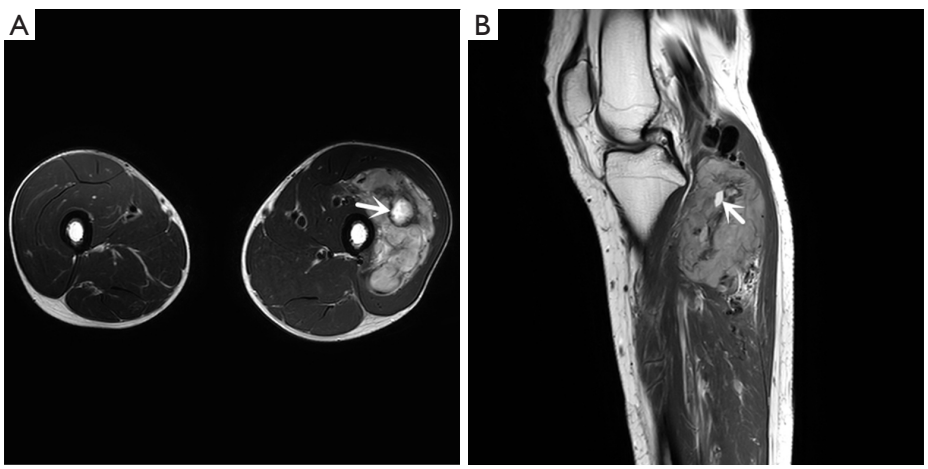

Figure 4 The axial (A) and sagittal (B) T1-weighted images of 3.0-T MRI scanner reveal the high signal intensity mass relative to muscle with internal hemorrhage (arrows). MRI, magnetic resonance imaging.

Figure 5 The coronal T2-weighted fat suppressed image of 3.0-T MRI scanner shows the mass manifesting high signal intensity compared to muscle (A), and the T1-weighted image (B) shows that the mass was hyperintense relative to muscle with intra- and extratumoral flow void vessels (arrows). MRI, magnetic resonance imaging.

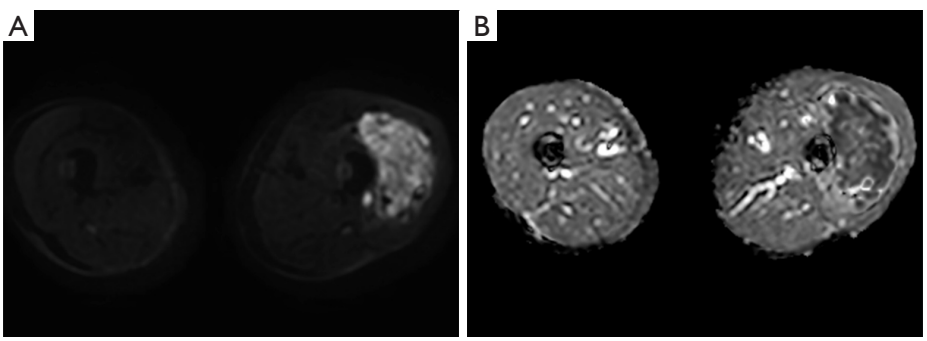

Figure 6 The axial DWI-weighted image at b=800 mm^2/s on 3.0-T MRI scanner shows a higher signal (A), and the corresponding gray-scale ADC map shows restriction (B). DWI, diffusion-weighted imaging; MRI, magnetic resonance imaging; ADC, apparent diffusion coefficient.

study showed that the median patient age at diagnosis was 23.50±6.36 years (9–49 years), and a majority (21/34) of the patients were aged less than 30 years. A total of 31 tumors were in the lower extremities, and 3 were located in the upper extremities. The male-dominated nature of our study (23:11) was somewhat different from the previous literature.

ASPS usually behaves as a slow-growing, painless mass with a long clinical course. Therefore, when patients first see a doctor, the tumor size is usually large, and distant metastasis has often occurred. The cancer tissue is rich in blood vessels; therefore, distant metastasis easily occurs through the hematogenous route, and lung metastasis is the most common, followed by brain, breast, and bone metastasis (16,17). In our series, the mean maximum diameter of the 34 masses was 8.70 cm, and 19/34 (55.9%) patients had metastases in both lungs at the time of the first diagnosis. These findings are consistent with the prior study reported by Yam *et al.* (17), which found that 62% of the patients had metastatic disease at presentation. In addition, 1 patient in our study developed pulmonary metastases 7 years after surgery, indicating the aggressiveness of ASPS. The metastatic tumor is the only significant poor prognostic factor (18). Long-term survival of patients without metastases at presentation is longer than those presenting with single or multiple sites of metastasis. Currently, radical surgical resection is the only validated standard treatment, as the views on adjuvant chemotherapy and auxiliary radiotherapy are controversial (14,16,18). Thus, early

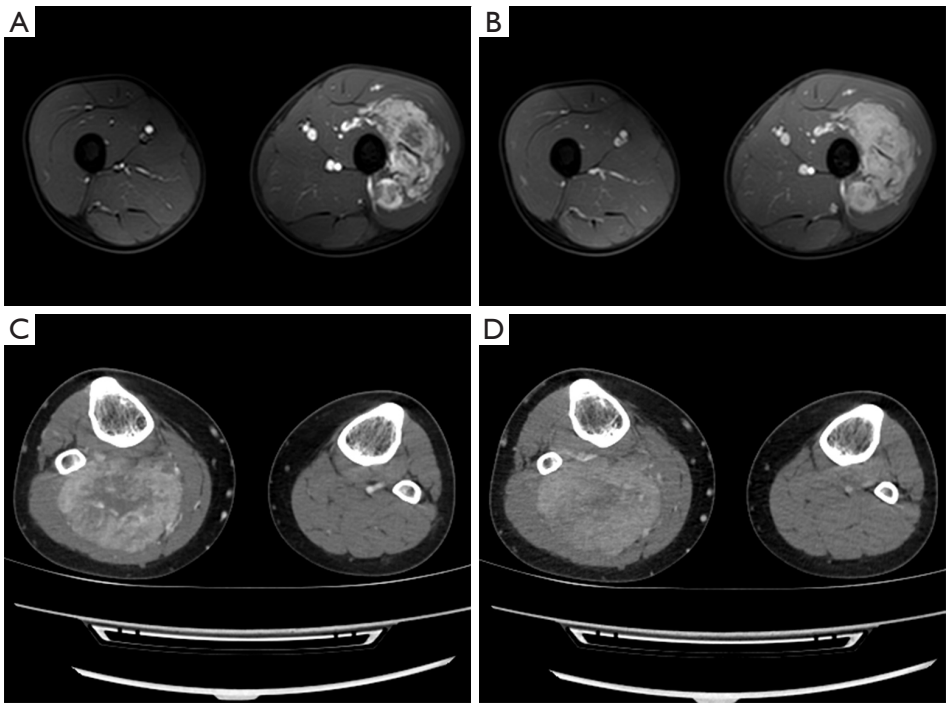

Figure 7 The DCE-MRI and CT findings of ASPS. The mass manifested early arterial enhancement at 2'3'' (A) and intense persistent enhancement at 4'22'' (B) on the DCE-MRI on 3.0-T MRI scanner, and the mass manifested intense persistent enhancement on the CT image (C,D). DCE-MRI, dynamic contrast enhanced-magnetic resonance imaging; CT, computed tomography; ASPS, alveolar soft part sarcoma.

diagnosis of ASPS with or without distant metastases is essential for therapeutic planning and improving prognosis.

ASPS is an extremely hypervascular mass surrounded by numerous enlarged and twisted vessels, which may present as a pulsatile mass with an audible bruit (5). MRI combined with contrast-enhanced MR angiography (MRA) is highly sensitive and specific in detecting arterial invasion in patients with musculoskeletal tumors, and the absence of ionizing radiation is a great advantage (19). In our retrospective study, the use of MRA was limited by cost, scanner availability, and level of expertise, and only 3 patients underwent CTA; CTA was found to clearly reveal the multiple tortuous and dilated blood vessels in and around the lesion, as well as the feeding arteries and draining veins of the tumor, even the abnormal channels between them. Moreover, MRI of the lung is challenging, so CT still represents the gold standard for the detection of lung metastases even if its sensitivity widely ranges in the literature since lung localizations are often atypical (20,21).

Compared with CT, MRI is the preferred imaging modality to assess this lesion due to its advantages of multisequence imaging capability and excellent soft tissue contrast. Previous studies have reported that, compared with adjacent muscles, ASPS exhibited isointensity or a slightly high signal intensity on T1WI, which was believed to be associated with the slow flow of blood in or around the tumors, and heterogenous hyperintensity on T2WI, which might be related to bleeding, necrosis, and scar formation in the tumor tissue (5,7,14). Furthermore, researchers have also noted that intra- and extra-tumoral vascular signal voids are frequently observed on MRI, which is attributed to tortuous and dilated vessels with rapid blood flow washout (22). Such flow voids or the high signal intensity on T1WI are not specific for ASPS, but the combination of them may represent the typical MRI features of ASPS. All the tumors in our cases demonstrated a slight hypersignal on T1WI, mixed high signal intensity on T2WI, and significantly high signal on FS sequences. In all cases, multiple intra- and peri-tumoral signal voids were also observed on all MR pulse sequences. These findings are consistent with the study by McCarville *et al.* (23) that the signal voids are primarily located at the superior and inferior poles of the neoplasms,

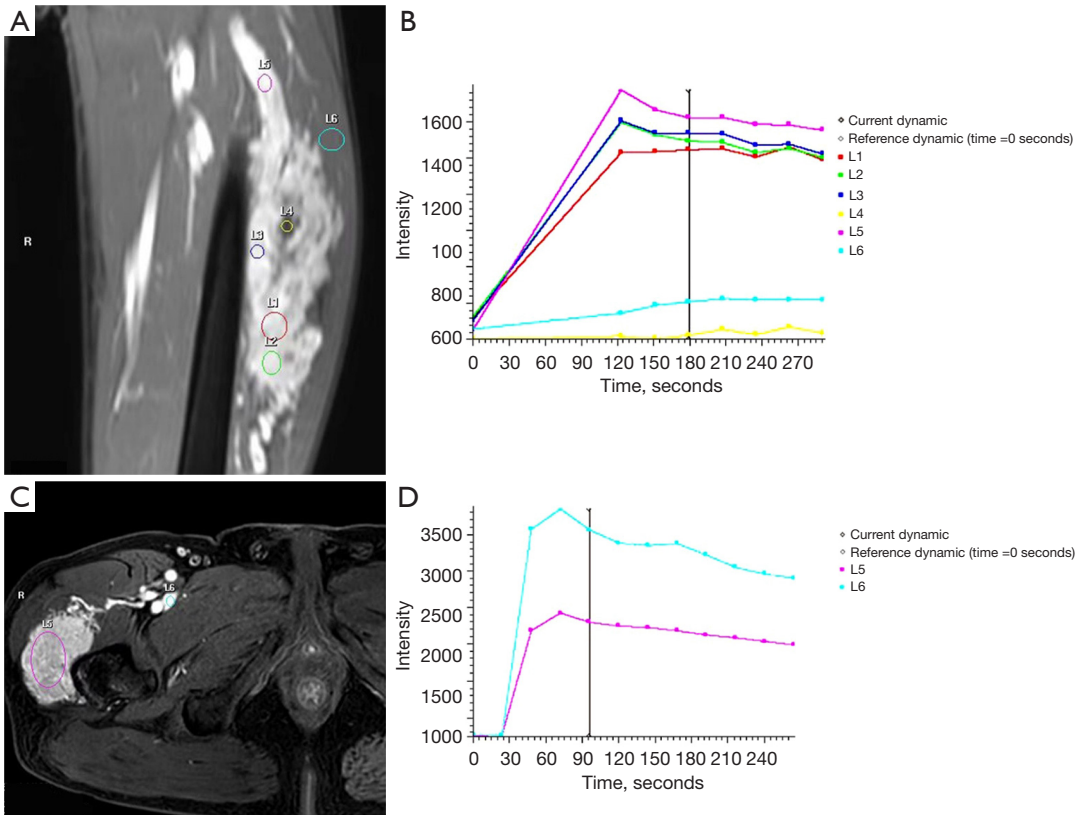

Figure 8 The TIC of ASPS on 3.0-T MRI scanner. (A,B) Male, 18 years old: (A) the placement of the region of interest on the raw image; (B) TIC, L1, L2, L3, and L5 represent lesions showing a rapid rise and slow washout type, L4 represents the internal hemorrhage, and L6 represents adjacent muscle. (C,D) Male, 49 years old: (C) the placement of the region of interest on the raw image; (D) the TIC of the L5 lesion shows a rapid rise and slow washout type, and L6 is the vessel. R, right; L1–6, line 1–6; ASPS, alveolar soft part sarcoma; TIC, time-intensity curve; MRI, magnetic resonance imaging.

Figure 9 CTA shows a large hypervascular mass with multiple enlarged tortuous vessels (arrow). CTA, computed tomography angiography.

which likely correspond to the feeding arteries and draining veins located primarily at the upper and lower poles of the lesion. As this is not clearly documented in the literature, future study may be beneficial. Conversely, the fibrovascular septa, which separated the nested cells, exhibited a linear low signal on T1WI and T2WI. McCarville *et al.* (23) also observed these thin dark bands on water-sensitive MR sequences.

In addition to T1WI and T2WI, other MRI techniques, including DCE and DWI, can provide information other than morphologic features to characterize malignant masses. Central necrosis, anatomic extent, and blood supply of the tumor can be detected through static contrast-enhanced MRI, but crucial information regarding tumor biology, vascular anatomy, and angiogenesis can only be assessed with DCE-MRI (24). TIC provides semi-quantitation of the tumor that reflects permeability and perfusion through

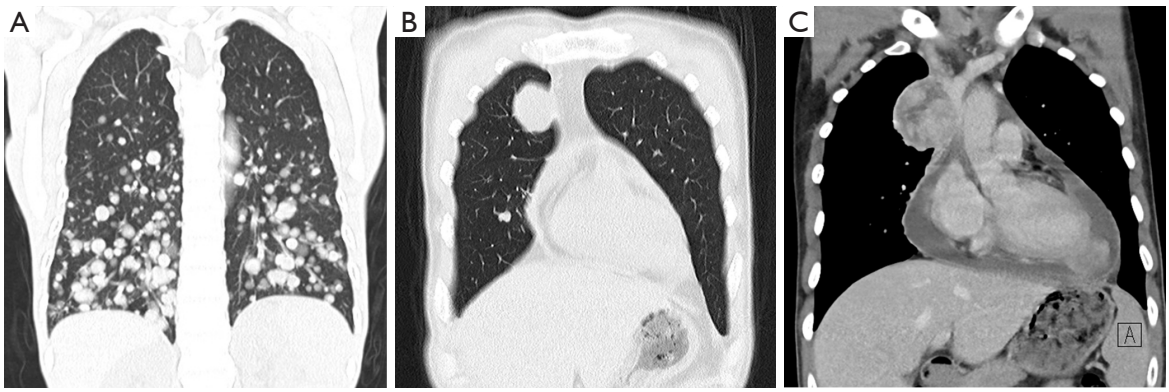

Figure 10 The CT images of lung metastasis. (A) Female, 48 years old, the coronal pulmonary window shows bilateral lung metastasis, predominating in the inferior lobes, at the initial visit. (B,C) Male, 30 years old: (B) the coronal pulmonary window; (C) the coronal mediastinal window in the venous phase; metastatic lung disease showed remarkable persistent enhancement. CT, computed tomography; A, anterior.

the enhancement pattern. Malignant soft tissue masses are characterized by increased capillary permeability, small interstitial spaces, and great angiogenesis. These masses demonstrate a typical enhancement pattern-early arterial enhancement, with rapid and high amplitude wash-in on DCE TIC (24,25). ASPS is highly vascularized, with small vascular spaces separating nests of cells. In this study, all the lesions were persistently remarkably enhanced on static contrast-enhanced MRI. A total of 23 masses demonstrated a typical enhancement pattern-early arterial enhancement followed by a slight decrease or slow washout, belonging to type III TIC (24,26). They were later confirmed to be malignant by pathology, which is consistent with previous research (27).

DWI is another MRI technique applied to the musculoskeletal system. Tissues with high cellularity, such as those with malignancy, tend to have decreased water motion or restricted diffusion and show high signal intensity on DWI and low ADC values compared to the adjacent skeletal muscle (28). A minimum ADC value of $\leq 1.0\times10^{-3}$ mm^2/s has been considered by several studies to be a clinically useful threshold for predicting malignant tumors (24,28). Del Grande *et al.* (29) further confirmed that DWI and ADC maps were indeed useful additions to conventional MRI, and the minimum ADC threshold for predicting malignancy was $\leq 0.8\times10^{-3}$ mm^2/s. Although only 12 of the 34 cases involved in our study undertook DWI, all of them exhibited hyperintensity on DWI with mean ADC values of $(0.86\pm0.07)\times10^{-3}$ mm^2/s, which was lower than those of previous reports (22,27). The discrepancy may be due to the difference in field strength, the number of signals averaged, and the anatomic ROI. For differential diagnosis, DWI and ADC values can be used as a noninvasive additional tool to differentiate ASPS from ES/ET, especially in borderline cases. Several studies have shown that the mean ADC values of ES/ET were $(0.71\pm0.16)\times10^{-3}$ or $(0.56\pm0.07)\times10^{-3}$ mm^2/s, lower than that of ASPS (30,31). ADC values are affected by the selection of the b-value and the extracellular environment of soft tissue tumors. So far, the selection of the optimal b-value is controversial and there is no standard method available to measure ADC values with respect to ROI size. Intravoxel incoherent motion (IVIM) MRI is based on a biexponential model of DWI, which can obtain both diffusion and perfusion parameters (24). At present, there are few studies about the application of IVIM to evaluate soft tissue tumors. In future, we will assess the value of ADC values in differentiating ASPS and other types of tumors and investigate the application of IVIM to improve ASPS diagnosis.

There were several limitations in this study. This study was a retrospective analysis and the observers were not blinded to the pathology diagnosis, which is likely to have caused some biases in characterization. Drawing the ROI with the largest soft tissue mass area on multiple slices may better reveal the ADC values of ASPS, but due to the intrinsic shortcoming of retrospective study and the limitation of the post-processing workstation in our center, that was not available to us. Due to the rarity of the tumor and that not all the patients underwent DCE-MRI and DWI, the sample size was modest and larger multicenter study is needed in the future. Molecular diagnosis was not performed in this study to reflect the ultrastructures of the

Table 3 Imaging features of patients

Imaging feature	Values
Margin	
Clear	28/34 (82.4)
Unclear	6/34 (17.6)
T1WI	
Hyperintensity signal	34/34 (100.0)
Thin hypodense bands	25/34 (73.5)
T2WI and fat-suppressed sequence	
Hyperintensity signal	34/34 (100.0)
Thin hypodense bands	25/34 (73.5)
Enhancement pattern	
Intense	23/23 (100.0)
Homogeneous	19/23 (82.6)
Peripheral	4/23 (17.4)
Flow voids	32/34 (94.1)
Intra-/peri-tumoral vessels	34/34 (100.0)
Value of CT artery phase (HU)	140.5±14.5 [120, 161]
DCE parameters	
Time to peak (s)	155.5±145.38 [48.1, 262.9]
Wash-in rate (L/s)	32.30±34.79 [5.4, 59.2]
Wash-out rate (L/s)	2.70±2.97 [0.2, 5.3]
Maximum enhancement (%)	945.55±313.88 [723.6, 1,667.6]
Maximum relative enhancement (%)	223.2 [155.0, 291.4]
ADC value ($\times 10^{-3}$ mm^2/s)	0.86±0.07 [0.6, 1.4]
Size (cm)	8.70±3.96 [3.0, 19.4]

Data are presented as number of tumors/total number (%), mean ± SD [range] or median [interquartile range]. T1WI, T1-weighted imaging; T2WI, T2-weighted imaging; CT, computed tomography; HU, Hounsfield unit; DCE, dynamic contrast enhanced; ADC, apparent diffusion coefficient; SD, standard deviation.

tumor, which would be a useful endeavor in the future.

The ADC values in our study were measured on an MRI scanner with different field strengths which may have influenced ADC mapping. Lastly, the imaging features of ASPS and ES/ET tumors were not compared side by side in this paper and further studies are needed in the future.

Conclusions

ASPS often manifests as a large, slow-growing mass and presents in the lower extremities of teenagers. The distinct imaging features of the hypersignal on T1WI and T2WI, flow voids, and multiple intra- and peri-tumoral feeding arteries and draining veins on CTA strongly suggested the presence of ASPS. Adding nonconventional MRI features, including early arterial enhancement on DCE TIC, high signal intensity on DWI, and low ADC values, can offer additional information on tumor biology and improve the overall accuracy of imaging diagnoses of ASPS.

Acknowledgments

Funding: None.

Footnote

Reporting Checklist: The authors have completed the MDAR reporting checklist. Available at https://qims.amegroups.com/article/view/10.21037/qims-23-743/rc

Conflicts of Interest: All authors have completed the ICMJE uniform disclosure form (available at https://qims.amegroups.com/article/view/10.21037/qims-23-743/coif). The authors have no conflicts of interest to declare.

Ethical Statement: The authors are accountable for all aspects of the work in ensuring that questions related to the accuracy or integrity of any part of the work are appropriately investigated and resolved. The retrospective study was approved by the Ethics Committee of Shaanxi Provincial People's Hospital (No. 2021X012). The study was conducted in accordance with the Declaration of Helsinki (as revised in 2013), and the requirement for informed consent was waived because of the study's retrospective nature.

References

1. Christopherson WM, Foote FW Jr, Stewart FW. Alveolar soft-part sarcomas; structurally characteristic tumors of uncertain histogenesis. Cancer 1952;5:100-11.
2. Sbaraglia M, Bellan E, Dei Tos AP. The 2020 WHO Classification of Soft Tissue Tumours: news and perspectives. Pathologica 2021;113:70-84.
3. Reis F, Macedo E, França Junior MC, Amstalden EI, Appenzeller S. Retroperitoneal Ewing's sarcoma/embryonal tumor: a rare differential diagnosis of back pain. Radiol Bras 2017;50:409-10.
4. Xu Z, Zhang Y, Yu YH. Successful treatment of advanced alveolar soft part sarcoma with camrelizumab combined with apatinib: a case report. Ann Palliat Med 2021;10:785-92.
5. Li X, Ye Z. Magnetic resonance imaging features of alveolar soft part sarcoma: report of 14 cases. World J Surg Oncol 2014;12:36.
6. Chen J, Chen X, Wang Y, Chen H, Wang Z. Imaging Findings and Histologic Appearances of Alveolar Soft Part Sarcoma in the Prostate: A Case Report and Review of the Literature. Clin Genitourin Cancer 2015;13:e315-e9.
7. Tian L, Cui CY, Lu SY, et al. Clinical presentation and CT/MRI findings of alveolar soft part sarcoma: a retrospective single-center analysis of 14 cases. Acta Radiol 2016;57:475-80.
8. Suh JS, Cho J, Lee SH, et al. Alveolar soft part sarcoma: MR and angiographic findings. Skeletal Radiol 2000;29:680-9.
9. Chen YD, Hsieh MS, Yao MS, Lin YH, Chan WP. MRI of alveolar soft-part sarcoma. Comput Med Imaging Graph 2006;30:479-82.
10. Gondim Teixeira PA, Renaud A, Aubert S, et al. Perfusion MR imaging at 3-Tesla: Can it predict tumor grade and histologic necrosis rate of musculoskeletal sarcoma? Diagn Interv Imaging 2018;99:473-81.
11. Zhu Y, Zhou Y, Zhang W, Xue L, Li Y, Jiang J, Zhong Y, Wang S, Jiang L. Value of quantitative dynamic contrast-enhanced and diffusion-weighted magnetic resonance imaging in predicting extramural venous invasion in locally advanced gastric cancer and prognostic significance. Quant Imaging Med Surg 2021;11:328-40.
12. Shapeero LG, Vanel D. Imaging evaluation of the response of high-grade osteosarcoma and Ewing sarcoma to chemotherapy with emphasis on dynamic contrast-enhanced magnetic resonance imaging. Semin Musculoskelet Radiol 2000;4:137-46.
13. Paoluzzi L, Maki RG. Diagnosis, Prognosis, and Treatment of Alveolar Soft-Part Sarcoma: A Review. JAMA Oncol 2019;5:254-60.
14. Zhang Y, Wang Y, Wang H, et al. Alveolar soft part sarcoma in childhood and adolescence: Report of three cases and review of literature. Front Pediatr 2022;10:937112.
15. Aksionau A, Dela Cruz NE, Meram AT, Cuellar-Saenz H, Aveni JR, Takei H. Lingual Alveolar Soft Part Sarcoma in a 78-Year-Old Woman: A Case Report and Comprehensive Review of the Literature from 1952 to 2022. Head Neck Pathol 2023;17:265-74.
16. Fujiwara T, Nakata E, Kunisada T, et al. Alveolar soft part sarcoma: progress toward improvement in survival? A population-based study. BMC Cancer 2022;22:891.
17. Yam MKH, Chan KKK. Alveolar soft part sarcoma in a young woman: A case report from Hong Kong. Radiol Case Rep 2022;17:1938-41.
18. Flores RJ, Harrison DJ, Federman NC, Furman WL, Huh WW, Broaddus EG, Okcu MF, Venkatramani R. Alveolar soft part sarcoma in children and young adults: A report of 69 cases. Pediatr Blood Cancer 2018;65:e26953.
19. Feydy A, Anract P, Tomeno B, Chevrot A, Drapé JL. Assessment of vascular invasion by musculoskeletal tumors of the limbs: use of contrast-enhanced MR angiography. Radiology 2006;238:611-21. Erratum in: Radiology 2007;242:950.
20. Branca RT, Cleveland ZI, Fubara B, Kumar CS, Maronpot RR, Leuschner C, Warren WS, Driehuys B. Molecular MRI for sensitive and specific detection of lung metastases. Proc Natl Acad Sci U S A 2010;107:3693-7.
21. Chiesa AM, Spinnato P, Miceli M, Facchini G. Radiologic Assessment of Osteosarcoma Lung Metastases: State of the Art and Recent Advances. Cells 2021;10:553.
22. Cui JF, Chen HS, Hao DP, et al. Magnetic Resonance Features and Characteristic Vascular Pattern of Alveolar Soft-Part Sarcoma. Oncol Res Treat 2017;40:580-5.
23. McCarville MB, Muzzafar S, Kao SC, Coffin CM, Parham DM, Anderson JR, Spunt SL. Imaging features of alveolar soft-part sarcoma: a report from Children's Oncology Group Study ARST0332. AJR Am J Roentgenol 2014;203:1345-52.
24. Ahlawat S, Fritz J, Morris CD, Fayad LM. Magnetic resonance imaging biomarkers in musculoskeletal soft tissue tumors: Review of conventional features and focus on nonmorphologic imaging. J Magn Reson Imaging 2019;50:11-27.
25. Noebauer-Huhmann IM, Amann G, Krssak M, et al. Use

of diagnostic dynamic contrast-enhanced (DCE)-MRI for targeting of soft tissue tumour biopsies at 3T: preliminary results. Eur Radiol 2015;25:2041-8.
26. Choi YJ, Lee IS, Song YS, Kim JI, Choi KU, Song JW. Diagnostic performance of diffusion-weighted (DWI) and dynamic contrast-enhanced (DCE) MRI for the differentiation of benign from malignant soft-tissue tumors. J Magn Reson Imaging 2019;50:798-809.
27. Oda T, Kikuchi K, Togao O, et al. Alveolar soft part sarcoma of the orbit: A case report. Radiol Case Rep 2021;16:3766-71.
28. Filograna L, Magarelli N, Cellini F, et al. Diffusion weighted imaging (DWI) and apparent diffusion coefficient (ADC) values for detection of malignant vertebral bone marrow lesions. Eur Rev Med Pharmacol Sci 2018;22:590-7.
29. Del Grande F, Ahlawat S, Subhawong T, Fayad LM. Characterization of indeterminate soft tissue masses referred for biopsy: What is the added value of contrast imaging at 3.0 tesla? J Magn Reson Imaging 2017;45:390-400. Erratum in: J Magn Reson Imaging 2017;45:1246.
30. Saleh MM, Abdelrahman TM, Madney Y, Mohamed G, Shokry AM, Moustafa AF. Multiparametric MRI with diffusion-weighted imaging in predicting response to chemotherapy in cases of osteosarcoma and Ewing's sarcoma. Br J Radiol 2020;93:20200257.
31. Parlak Ş, Ergen FB, Yüksel GY, Karakaya J, Aydın GB, Kösemehmetoğlu K, Aydıngöz Ü. Diffusion-weighted imaging for the differentiation of Ewing sarcoma from osteosarcoma. Skeletal Radiol 2021;50:2023-30.

Cite this article as: Lv C, Xue X, Huang M, Yang Z, Chen X, Koo CW. The dynamic contrast enhanced-magnetic resonance imaging and diffusion-weighted imaging features of alveolar soft part sarcoma. Quant Imaging Med Surg 2023;13(10):7269-7280. doi: 10.21037/qims-23-743

